J Appl Electrochem (2011) 41:535–541
DOI 10.1007/s10800-011-0263-6

ORIGINAL PAPER

Study of the effect of new brightener on Zn–Ni alloy electrodeposition from acid sulphate bath

S. Basavanna · Y. Arthoba Naik

Received: 24 September 2010 / Accepted: 10 February 2011 / Published online: 2 March 2011

Abstract The electrodeposition of Zn–Ni alloy from acid sulphate bath was carried out in presence of a brightener, such as condensation product of vanillin and serine (VS). The cyclic voltammetry and chronoamperometry techniques were used to study the nucleation mechanism process, while polarization and electrochemical impedance spectroscopic (EIS) techniques for corrosion studies. The model of Scharifker and Hills was used to analyze the current transients and it revealed that Zn–Ni electrocrystallization process in presence of VS, under the studied conditions, is governed by progressive nucleation process. Corrosion studies showed that bright Zn–Ni alloy coatings exhibited higher corrosion resistant nature. The Zn–Ni layer obtained in presence of VS shows smooth morphology with smaller grain sizes and higher percentage of reflectance signals.

Keywords Electrodeposition · Brightener · Nucleation · Reflectance · Zn–Ni alloy

1 Introduction

Zinc alloy deposition has been of interest recently since such alloys provide better corrosion protection than electrogalvanized coatings [1]. Electroplated binary Zn–M alloys, where M is an iron-group metal (Fe, Co or Ni), exhibit improved properties compared to pure Zn [2]. Zn–Ni coatings have been formed by galvanostatic [3, 4], pulse plating [5] and as composition modulated alloys [6]. Zn–Ni layers provide good protection for steel, and the maximum protective ability is reached with a Ni content up to 14%, which depends on bath composition and operating conditions [7, 8]. The electrodeposition of Zn–Ni alloys is classified by Brenner [9] as an anomalous codeposition, where zinc, which is the less noble metal, is preferentially deposited. Although this phenomenon [10] has been known since 1907, the codeposition mechanisms of zinc and nickel are not well understood [11, 12]. There are some propositions to explain the anomalous codeposition of Zn–Ni alloys. The first attributes the anomalous codeposition to a local pH increase, which could induce zinc hydroxide precipitation and would inhibit nickel deposition [13]. Several models have been suggested to explain the anomalous codeposition of zinc alloys [14–16].

There are broadly two types of plating baths for Zn–Ni alloy, namely the acid type [17, 18] and the alkaline type [19, 20]. The acid bath consists of a mixture of zinc and nickel salts, electrolytes, buffers and optional brighteners. Weak acid electrolytes operating at high current densities yield Zn–Ni deposits with the relatively low nickel content (normally 5–10 at.%) and non-uniform nickel distribution throughout the coating. In the alkaline type, the electrolyte consists of NaOH and additives to maintain the metal species in solution. In contrast, alkaline baths, which can ensure normal nickel plating, yield more uniform coatings with much higher nickel content as compared to acid baths (and, therefore, with enhanced corrosion resistance); however, these baths operate at low current densities [21].

The use of additives in electrolytic baths is very important due to their influence on the growth and structure of the deposits obtained. Typically, additives are added to the electrolytic bath at concentrations on the order of parts per million; their presence in the bath promotes the formation of smooth and shiny coatings [22–24]. Additive molecules

S. Basavanna · Y. Arthoba Naik (✉)
Department of Chemistry, School of Chemical Sciences, Kuvempu University, Shankaraghatta 577451, India
e-mail: drarthoba@yahoo.co.in

adsorbed on the cathode surface can affect the activation energy [25] and the rate of charge transfer in the electrochemical reaction, and may also influence the mechanism of electrocrystallization. In addition, the adsorbed additives block part of the electrode surface, thereby reducing the number of active sites for the formation of nuclei and causing a decline in the nucleation rate [26, 27].

In the present work, investigation of new brightener for Zn–Ni alloy coatings has been undertaken with an emphasis on surface morphology, phase structure and corrosion behaviour of the deposits. In addition, the nucleation mechanism of electrodeposition in presence and absence of brightener were studied.

2 Experimental

All the bath compositions for Zn–Ni deposits are given in Table 1. The bath solutions were freshly prepared using analytical grade chemicals in double distilled water, and used for the experiments without further purification.

The standard Hull cell of 267 mL capacity was used to optimize the bath constituents. The Hull cell experiments were carried out without agitation. The pH of the solution was adjusted with 10% H_2SO_4 or sodium bicarbonate solution. Zinc plate of 99.99% purity was used as anode. The anode was activated each time by immersing in 10% HCl followed by water wash. Mild steel plates (AISI-1079) of standard Hull cell size were mechanically polished to obtain a smooth surface and degreased by dipping in boiling trichloroethylene. The scales and dust on the steel plates were removed by dipping in 10% HCl solution and were subjected to electrocleaning process. After this the steel plates were washed with water and used for the experiment as such. After Hull cell experiment the plate was removed from the solution and subjected to bright dip in 1% nitric acid for 3–5 s followed by water wash.

The condensation product was prepared from 1:1 amounts of vanillin and serine in ethanol medium (50 mL), under reflux condition for 3 h at 343 K [28]. The completion of the reaction was confirmed by TLC. The obtained solution was made up to 100 mL using double distilled water and the same was used for the experiments.

Table 1 Optimum bath composition and operating conditions

Bath composition	Concentration (mol L^{-1})	Operating conditions
$ZnSO_4 \cdot 7H_2O$	0.5	pH: 3.5
$NiSO_4 \cdot 6H_2O$	0.1	Temperature: 298 K
Na_2SO_4	0.2	Bright current density range: 1.0–5.0 A dm^{-2}
H_3BO_3	0.2	Anode: zinc plate (99.99%)
CTAB	0.003	Cathode: mild steel
VS (mL L^{-1})	25	

The cyclic voltammetric and chronoamperometric studies were performed using CHI660D electrochemical workstation with a three electrode system. A steel electrode of geometrical area 0.07 cm^2, a platinum wire and saturated calomel were used as working, counter and reference electrodes, respectively. Prior to each experiment, the working electrode was polished to a mirror finish with 0.05 μm alumina.

The potentiodynamic polarization and electrochemical impedance studies (EIS) were carried out in a typical three electrode system with the coated mild steel electrode (area 1 cm^2) used as working electrode. The corrosion behaviour of Zn–Ni alloy coatings of thickness 10 μm, obtained from the optimized bath in presence and absence of vanillin and serine (VS) was measured in 3.5 wt% NaCl solution. The composition and surface morphology of deposits on mild steel electrodes (2 × 2 cm^2) were examined using an EDX analyser integrated with scanning electron microscope (JEOL-JSM-6400). The Philips X'pert PRO MPD X-ray diffractometer was used to determine the Zn–Ni alloy phases present in the deposits.

The percentage reflection of deposits was determined using Ocean optics USB 4000 Spectrophotometer, referenced against a vacuum coated silver mirror. The reflectivity of silver mirror was set at 100% and measurements were carried out at different surface points of the deposited samples.

3 Results and discussions

3.1 Electrodeposition

The Hull cell was used to optimize the bath composition containing zinc sulphate, sodium sulphate, CTAB and boric acid. The CTAB was used as a wetting agent in the deposition process. The basic bath gave coarse dull deposit between the current density range of 0.5–3.5 A dm^{-2}. In order to improve the nature of the deposit, known volume of VS was added to the bath solution. Similar to our earlier studies [29–31], the effect of bath constituents, pH, current density and temperature were optimized. The optimum bath compositions and operating parameters are represented in Table 1. The optimized bath solution gave mirror bright deposits of between the current density range of 1–5 A dm^{-2}.

3.2 Cyclicvoltammetric studies

The influence of VS on codeposition of Zn–Ni alloy was studied using cyclicvoltammetric technique. Figure 1

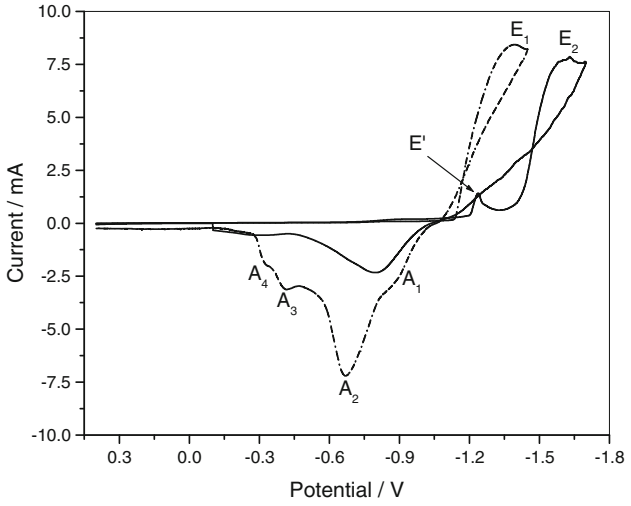

Fig. 1 Typical cyclic voltammograms obtained in presence (*solid line*) and absence (*dashed line*) of VS in the bath solution

shows typical cyclic voltammograms obtained from the optimized bath solution in presence and absence of VS.

In absence of VS in the optimized bath solution, the voltammogram shows one cathodic and four oxidation peaks (A_1, A_2, A_3 and A_4). The detection of multiple peaks during the electrochemical oxidation of alloys can be attributed to the dissolution of metals in the alloy via different intermediate phases [32]. Thus, the voltammetric response gives information regarding the components of the alloy and structure of the deposited phases.

The four anodic peaks (A_1 to A_4) corresponding to the dissolution of three phases of Zn–Ni alloy deposit are η-phase, δ-phase (Ni_3Zn_{22}) and γ-phase (Ni_5Zn_{21}). The first peak (A_1) at a potential of -0.9 V corresponds to the oxidation of zinc from the η-phase, the phase with a very low nickel content, which is almost pure zinc phase. The second peak (A_2) at a potential -0.67 V and third peak (A_3) at a potential (-0.41 V) corresponding to the dissolution of zinc from δ- and γ-phases, respectively. The fourth peak (A_4) at more noble potential characterizes the dissolution of nickel from η, γ and δ phases [33, 34].

The two cathodic peaks (E' and E_2) observed during the reduction of zinc ions in presence of VS, associated with the partial adsorption of additive on the steel surface. When additive adsorbs on the electrode surface, it blocks a fraction of the active sites ($\theta_{blocked}$) at which the first reduction process occurs [35]. As a result, the reduction of zinc ions occurs only at the fraction of active sites ($1 - \theta_{blocked}$) that are not blocked. Thus, the current density associated with the reduction of zinc ions decreases with respect to that observed in the absence of VS. When an increase in the overpotential, desorption of additive takes place, allowing the reduction of zinc ions at the active sites. When the potential scan is reversed, two anodic peaks with a decreasing peaks intensity are observed correspond to the dissolution of zinc and nickel from η and γ phases. These results indicated that the VS partially adsorb on the steel surface and decreases the reduction process and enhances the formation of more compact bright deposits.

3.3 Transient analysis

The chronoamperometric studies were used to identify the Zn–Ni nucleation mechanism at different potentials. This potentiostatic technique has proved to be a powerful tool for elucidating the mechanisms by which new phases form (electrocrystallization) [36]. For most of the metals, the charge transfer rate is sufficiently high and the continued growth of formed nuclei is entirely mass-transfer-controlled, two limiting cases of multiple nucleations with diffusion-controlled growth can be conventionally considered depending on the nucleation rate, in accordance with the theory.

In the first case, at high nucleation rates, all nuclei are formed immediately after the potential step and their number remains constant during the growth process. This case is considered as instantaneous nucleation and is described by

$$I(t) = [zFD^{1/2}c/(\pi t)^{1/2}][1 - \exp(-N)] \quad (1)$$

where $I(t)$ is current density related to the geometric area of the electrode surface, N the total number of the formed nuclei, k the numerical constant calculated from

$$k = (8\pi cM/\rho)^{1/2} \quad (2)$$

M and ρ are the molar mass and the density of deposited metal, zF the molar charge of the electrodepositing species, D the diffusion coefficient, c the bulk concentration (in mol dm^{-3}).

In the second case, at small nucleation rates, when the nuclei are continuously formed during the whole time window before overlapping of diffusion hemispheres around the growing nuclei, is called progressive nucleation [36]. In this case metal clusters of different sizes can be formed, especially at the very initial time (t). The current transients for the progressive three-dimensional nucleation-growth mechanism are given by

$$I(t) = [zFD^{1/2}c/(\pi t)^{1/2}][1 - \exp(-aN_0'Dt^2/2)] \quad (3)$$

where N_0 is the number density of substrate active sites, a is the steady-state nucleation rate constant per site, k' is a numerical constant given by

$$k' = 4/3(8\pi cM/\rho)^{1/2} \quad (4)$$

Figure 2 shows the potentiostatic current versus time (I–t) transients recorded during the reduction of Zn–Ni

alloy in the potential range from −1.14 V to −1.38 V in absence of VS and −1.44 to −1.64 V in presence of VS in the optimized bath solution. The behaviour of these transients is typical of a nucleation process with three-dimensional growth of nuclei limited by the diffusion of the electroactive species. Each of the transients in Fig. 2 exhibit an increase in current density up to a maximum followed by a decay that converges to the limiting current, which corresponds to linear diffusion of the electroactive ions to a planar electrode. The anomalous behaviour observed at lower potentials (Fig. 2b) may be attributed to the adsorption of brightener on the electrode surface which alters the limiting current.

In order to characterize the nucleation process, the current transients were normalized to $(I/I_{max})^2$ versus t/t_{max} and then compared to the well known theoretical $(I/I_{max})^2$ versus t/t_{max} curves derived for instantaneous and progressive three-dimensional (3D) nucleation/growth models [31], whose equations are given for instantaneous nucleation

$$\left(\frac{I}{I_{max}}\right)^2 = \frac{1.9542}{t/t_{max}}\left\{1 - \exp\left[-1.2564\left(\frac{t}{t_{max}}\right)\right]\right\}^2 \quad (5)$$

and for progressive nucleation

$$\left(\frac{I}{I_{max}}\right)^2 = \frac{1.2254}{t/t_{max}}\left\{1 - \exp\left[-2.3367\left(\frac{t}{t_{max}}\right)^2\right]\right\}^2 \quad (6)$$

Nondimensional plots obtained with the experimental and theoretical data for Zn–Ni alloy deposition in the absence and presence of VS are shown in Fig. 3 at different potentials. Figure 3a and b shows that experimental $(I/I_m)^2$ curve is much larger than the theoretical model after the time maximum (t_{max}). The following mechanism explains the anomalous behaviour of iron-group metal ions on the electrode surface [37].

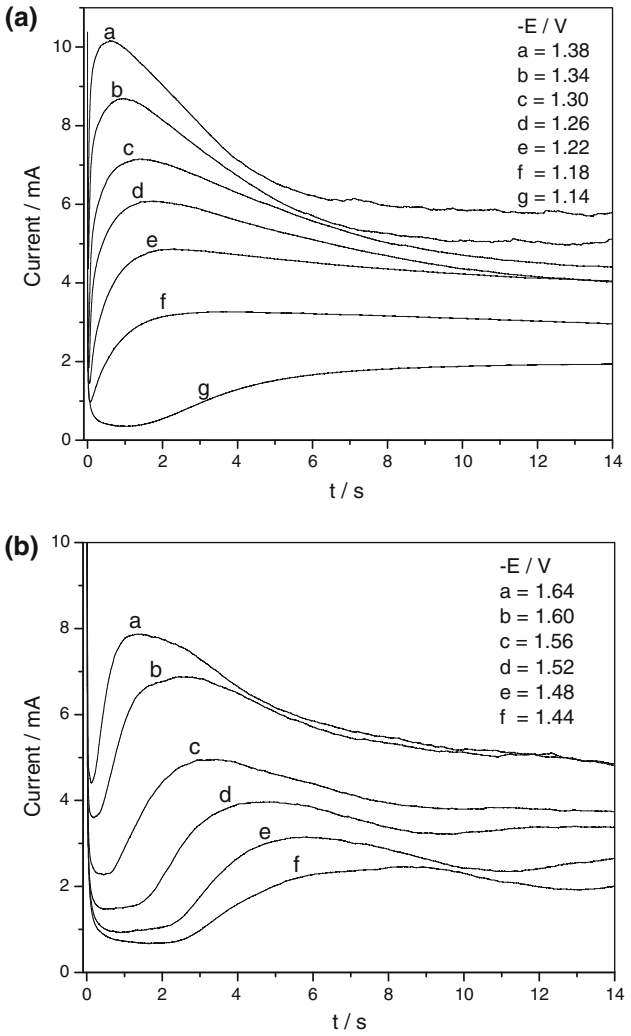

Fig. 2 Current transients for Zn–Ni deposition from optimized bath: **a** in absence and **b** in presence of VS

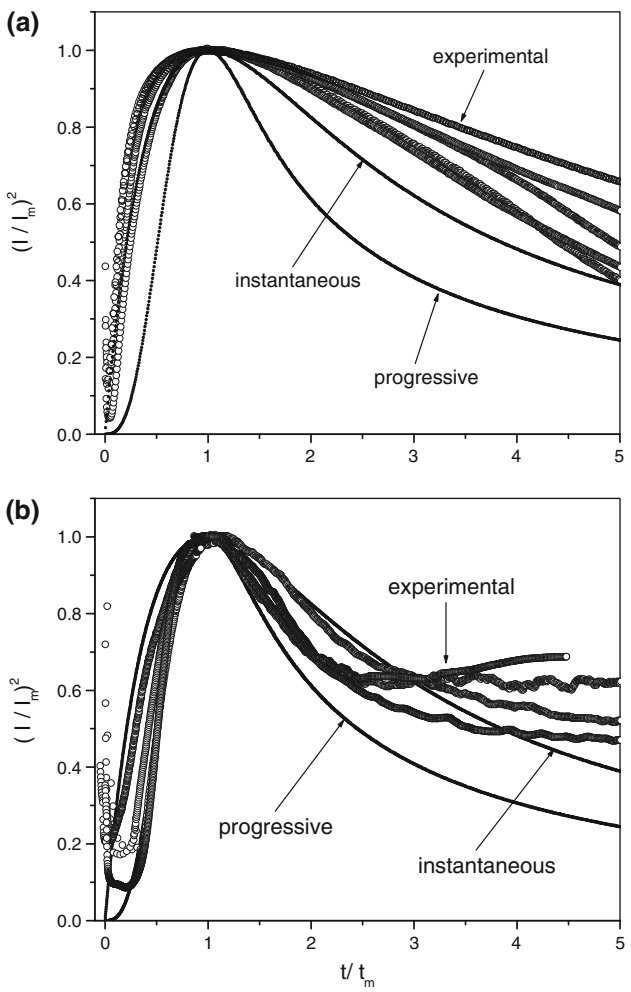

Fig. 3 Non-dimensional j/j_{max} versus t/t_{max} plot for electrodeposition of Zn–Ni alloy coating: **a** in absence and **b** in presence of VS

$$2H_2O + 2e^- \rightarrow H_2 + 2OH^- \quad (7)$$

$$M^{2+} + OH^- \rightarrow M(OH)^+ \quad (8)$$

$$M(OH)^+ \rightarrow M(OH)^+_{ads} \quad (9)$$

$$M(OH)^+_{ads} + 2e^- \rightarrow M + OH^- \quad (10)$$

where M designates iron, cobalt and nickel atoms. The reduction rate of M mainly depends on the stability of $M(OH)^+_{ads}$ or $M(OH)^+$. The stability of the zinc and nickel metal monohydroxide ions or metal hydroxides can be sorted in the following order: $Ni(OH)^+ > Zn(OH)^+$. As elucidated above, the content of nickel in the electrodeposit is much lower than that in the electroplating solution and the concentration of Ni^{2+} in the vicinity of the cathode should maintain a relatively steady value during the whole electroplating process. Meanwhile the nucleation/growth process of Zn–Ni deposit was always coupled with the evolution of hydrogen, which can be seen from Eqs. 7 and 10. Consequently, the experimental $(I/I_m)^2$ should be much larger than the theoretical model [34].

In Fig. 3a, the rising part of the transients are located on instantaneous nucleation curve at higher potentials. At lower potential the normalized curve is located between theoretical progressive and instantaneous nucleation. As soon as the potential changes to more negative values, the nucleation process confirms the instantaneous nucleation process. These results confirm that as soon as zinc being incorporated to the deposits the nucleation process is modified. Figure 3b shows the nucleation mechanism of Zn–Ni alloy deposition obtained in presence of VS. The normalized curves are located on theoretical progressive nucleation curve under studied potentials. These results confirmed that the nucleation process occurs by progressive nucleation in presence of VS in the bath solution.

Another diagnosis criterion given by the Schrifker and Hills nucleation model is based on the rising portion of the transient of current–time curve, in other words, on the analysis of the early stages of deposition [36]. It is possible to represent I versus $t^{1/2}$ for instantaneous, and I versus $t^{3/2}$ for progressive nucleation. Figure 4a shows the plots of I versus $t^{1/2}$ fitted linearly in absence of VS attributed the nucleation mechanisms occurs by instantaneous nucleation. In Fig. 4b, a better degree of linearity is obtained for I versus $t^{3/2}$ plot obtained in presence of VS, confirms a progressive nucleation mechanism occurs under the experimental conditions.

3.4 Impedance and polarization studies

The electrochemical behaviours of electrodeposited Zn–Ni alloys were studied using impedance spectroscopy. Figure 5a presents the comparison of Nyquist plots of Zn–Ni alloy

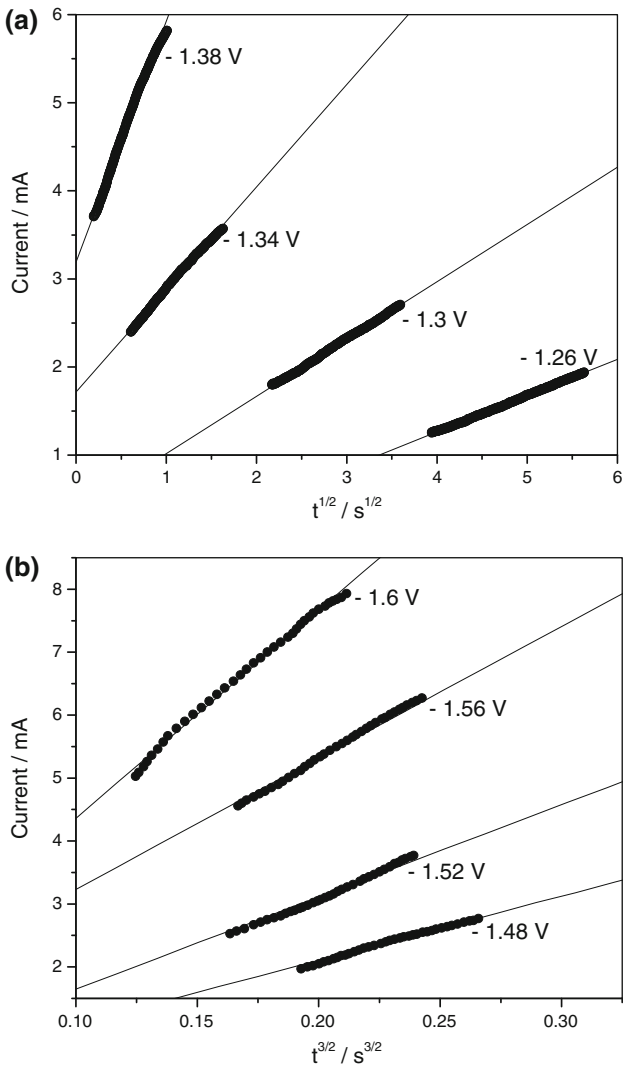

Fig. 4 Dependence between **a** I versus $t^{1/2}$ plots for initial transient portion from Fig. 2a and **b** I versus $t^{3/2}$ plots for initial transient portion from Fig. 2b

deposits obtained in absence and presence of VS in the bath solution. The R_{ct} value of deposits obtained in absence and presence of VS was about 33.54 and 102.3 Ω/cm^2, respectively. This behaviour suggests that the bright coating reduces the ion diffusion process and can reduce the corrosion rate of the substrate. This is in a good agreement with the results of potentiodynamic polarization investigations.

Figure 5b shows Tafel curves for the dull and bright coatings on mild steel samples. The I_{corr} value of bright deposit was 1.03 mA/cm^2 as against 2.36 mA/cm^2 for dull deposit. These results indicated that the bright deposit can act as a protective layer and improve the corrosion resistance of mild steel substrates in simulated physiological environment.

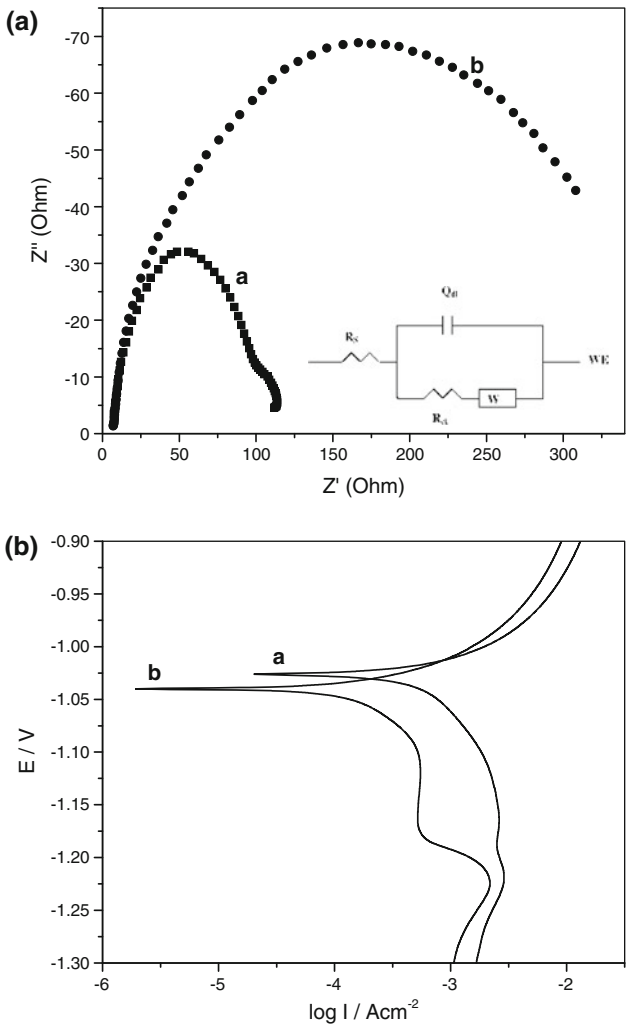

Fig. 5 **a** Nyquist impedance plots, **b** Tafel polarization curves of Zn–Ni alloy coatings in 3.5 wt% NaCl solution. The electrodeposits obtained *a* in absence and *b* in presence of VS in the bath solution

3.5 SEM and reflectance studies

The nature of crystal growth in presence and absence of VS is explained with the help of SEM photomicrographs (Fig. 6). The SEM photomicrographs of the deposits are obtained from the optimized bath solution. Figure 6a shows coarse-grained deposit having non-uniform crystal size obtained in absence of VS. In presence of VS in the bath solution increases the refinement of crystal size, regulates the uniform arrangement of crystals and hence results in the mirror bright deposits (Fig. 6b).

The ideal reflectance and the degrees of total reflection as a function of wavelength of visible light for the Zn–Ni alloy electrodeposits in presence and absence of VS are shown in Fig. 7. It can be seen from the Fig. 7 that the addition of VS into the bath solution led to an increase in the degree of mirror reflection in the visible region. Only of 3–5% variation in the total reflectance was observed at different surface points of Zn–Ni alloy coatings. These results confirmed that VS acts as a good brightener for Zn–Ni alloy coatings.

3.6 X-ray diffraction (XRD) analysis

The XRD patterns show (Fig. 8) the formation of lines corresponding to η-phase Zn (101) and additional lines that can be indexed considering a γ-Ni_5Zn_{21} and δ-Ni_3Zn_{22} phases. All the peaks are corresponding to the Zn and Zn–Ni alloy only, indicated that the deposits are free from impurities. In addition, an increase is observed in the intensity of γ-Ni_5Zn_{21} phase lines obtained in presence of VS in the bath solution. The increase in the intensity of γ-Ni_5Zn_{21} phase lines attributed to the increase in the percentage of Ni. These results are in good agreement with the EDX analysis of the deposits. EDX analysis shows that the percentage of Ni in absence and presence of VS in the bath solution is 1.8% and 2.5%, respectively. The average grain size of the deposits calculated using Scherrer equation was found to be 40 nm and 80 nm, in presence and absence of brightener in the bath solution, respectively.

4 Conclusions

The decorative Zn–Ni alloy coatings were prepared in presence of VS from the acid sulphate bath. The voltammetric studies showed that the reduction peak potential

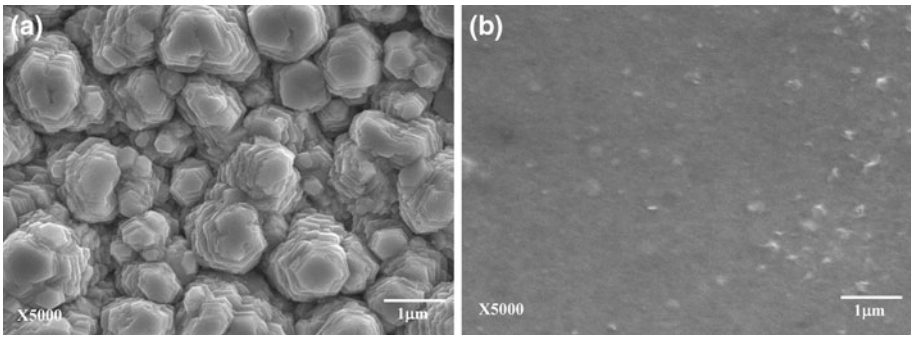

Fig. 6 SEM images of Zn–Ni coatings electrodeposited at current density 4 A dm^{-2}: **a** in absence and **b** in presence of VS in the bath solution

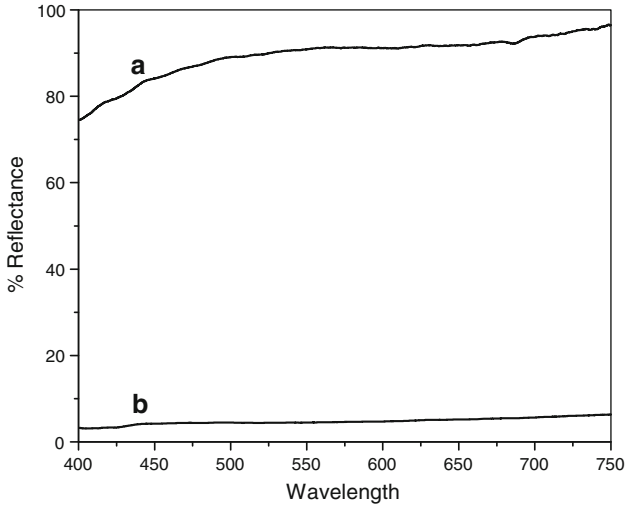

Fig. 7 The reflectance spectra for Zn–Ni alloy coatings electrodeposited at current density 4 A dm^{-2}: (*a*) in presence and (*b*) in absence of VS in the bath solution

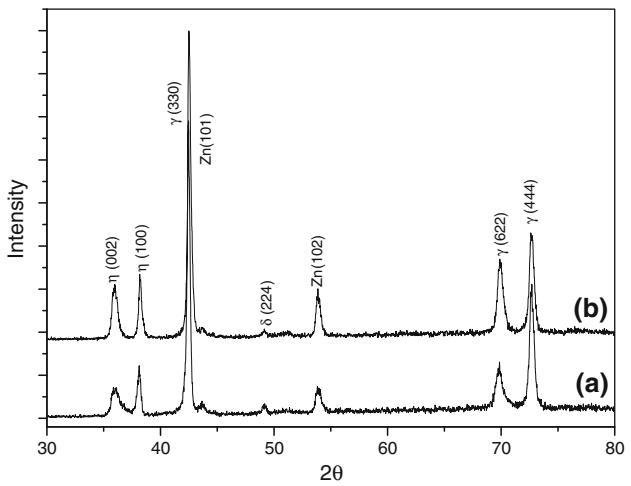

Fig. 8 X-ray diffraction patterns of electrodeposits of Zn–Ni alloy (*A*) in absence and (*B*) in presence of VS

shifts towards more negative direction and presence of anodic peaks for different Zn–Ni alloy phases in the deposits. Chronoamperometric studies showed that electroplating of Zn–Ni alloy in presence of VS follows 3D nucleation and subsequent progressive crystal growth mechanism. Corrosion studies revealed that the optimized bath in presence of VS yields high corrosion resistant Zn–Ni coatings. SEM and reflectance measurements confirmed the formation of fine-grained deposits in presence of additive, promoting the formation of smooth and bright coatings.

Acknowledgment The authors are grateful to the Kuvempu University, Department of Science & Technology and University Grants Commission, New Delhi, for providing the laboratory facilities to carryout this work.

References

1. Hall DE (1983) Plat Surf Finish 70:59
2. Wang ZL, Yang YX, Chen YR (2005) J Corros Sci Eng 7:18
3. Chandrasekar MS, Srinivasan S, Pushpavanam M (2009) J Solid State Electrochem 13:781
4. Soares ME, Souza CAC, Kuri SE (2006) Surf Coat Technol 201:2953
5. Ramanauskas R, Gudaviciute L, Kalinicenko A, Juskenas R (2005) J Solid State Electrochem 9:900
6. Ivanov I, Kirilova I (2003) J Appl Electrochem 33:239
7. Gavrila M, Millet JP, Mazille H, Marchandise D, Cuntz JM (2000) Surf Coat Technol 123:164
8. Garcia J, Barcelo G, Sarret M, Muller C, Pregonas J (1994) J Appl Electrochem 24:1249
9. Brenner A (1963) Electrodeposition of alloys, vol 1. Academic Press, New York
10. Shoch EP, Hirsch A (1907) J Am Chem Soc 29:314
11. Swathirajan S (1987) J Electroanal Chem 221:211
12. Mathias MF, Chapman TW (1990) J Electrochem Soc 137:102
13. Higashi K, Fukushima H, Takayushi V, Adaniya T, Matsudo K (1981) J Electrochem Soc 128:2091
14. Bahrololoom ME, Gabe DR, Wilcox GD (2003) J Electrochem Soc 150:C144
15. Lichusina S, Chodosovskaja A, Sudavicious A, Juskenas R, Bucinskiene D, Selskis A, Juzeliunas E (2008) Chemija 19:25
16. Ortiz-Aparicio JL, Meas Y, Trejo G, Ortega R, Chapman TW, Chainet E, Ozil P (2007) Electrochim Acta 52:4742
17. Fabri Miranda FJ, Barcia OE, Diaz SL, Mattos OR, Wiart R (1996) Electrochim Acta 41:1041
18. Pushpavanam M, Balakrishanan K (1996) J Appl Electrochem 26:283
19. Danilov FI, Shevlyakov IA, Sknar TE (1999) Russ J Electrochem 35:1033
20. Lee HY, Kim SG (2000) Surf Coat Technol 135:69
21. Bates JA (1994) Plat Surf Finish 81:36
22. Muralidhara HB, Arthoba Naik Y, Sachin HP, Venkatesha TV (2008) Indian J Chem Technol 15:155
23. Arthoba Naik Y, Venkatesha TV (2005) Bull Mater Sci 28:495
24. Muralidhara HB, Arthoba Naik Y (2008) Surf Coat Technol 202(14):3403
25. Kelly JJ, West AC (1998) J Electrochem Soc 145:3472
26. Bonou L, Ayraud M, Denoyel R, Massiani Y (2002) Electrochim Acta 47:4139
27. Moffat TP, Wheeler D, Josell D (2004) J Electrochem Soc 151:C262
28. Chen D, Martell AE (1987) Inorg Chem 26:1026
29. Muralidhara HB, Arthoba Naik Y, Venkatesha TV (2006) Bull Mater Sci 29:497
30. Muralidhara HB, Arthoba Naik Y, Sachin HP, Ganesha Achary, Venkatesha TV (2008) Indian J Chem Technol 15:259
31. Shivakumara S, Sachin HP, Ganesha Achary, Arthoba Naik Y, Venkatesha TV (2006) Bull Electrochem 22:371
32. Jovic VD, Zejnilovic RM, Despic AR, Stevanovic JS (1998) J Appl Electrochem 18:511
33. Abou-Krisha MM (2005) Appl Surf Sci 252:1035
34. Basavanna S, Arthoba Naik Y (2009) J Appl Electrochem 39:1975
35. Ballesteros JC, Dıaz-Arista P, Meas Y, Ortega R, Trejo G (2007) Electrochim Acta 52:3686
36. Scharifker BR, Hills G (1983) Electrochim Acta 28:879
37. Tsay P, Hu CC (2002) J Electrochem Soc 149:C492